Being positive isn't everything – exploring selectivities and affinities of a self-assembled, multiple redox-state, receptor that binds anions with up to picomolar affinities.

Ahmed Zubi,[†▲] Simon Turega,[‡] Igor Marques,[§] José R. B. Gomes,[§] Vítor Félix,[§*] and Jim A Thomas[†*]

[†]Department of Chemistry, University of Sheffield, Brook Hill, Sheffield, S3 7HF, UK.

[‡]Department of Bioscience and Chemistry, Sheffield Hallam University, Howard Street, Sheffield, S1 1WB, UK

[§]Department of Chemistry, CICECO – Aveiro Institute of Materials, University of Aveiro, 3810-193, Aveiro, Portugal.

ABSTRACT: (Word Style "BD_Abstract"). All manuscripts must be accompanied by an abstract. The abstract should briefly state the problem or purpose of the research, indicate the theoretical or experimental plan used, summarize the principal findings, and point out the major conclusions. Abstract length is one paragraph.

Introduction

As anions have important roles in a spectrum of areas within biology and the environment, their detection is an increasingly important research subject. As a consequence, the coordination chemistry of anions and their binding by specifically designed receptors and sensors has burgeoned over the last two decades. However, the difficulties inherent in the non-covalent recognition of anions are well rehearsed: compared to analogous cations they are larger and have lower charge densities, possess a wider spectrum of shapes, may only exist within a specific pH range, and tend to have higher free energies of solvation.

For these reasons, macrocyclic structures are frequently targeted in the construction of anion receptors as these architectures often display greater selectivities and higher affinities than other host designs. Furthermore, if these hosts are optically or electrochemically active, so that they can supply an output for the recognition process, they can also function as sensors for their anionic guests. The difficulty in this approach lies in the challenging syntheses required to isolate such complex structures. An alternative approach that has been much pursued involves self-assembly, with metal ion-directed approaches being particularly fruitful.

Another area of coordination chemistry research that has a longer history is focused on mixed-valence, MV, transition metal complexes. Through experimental and theoretical work, MV systems have been intensely studied for approximately fifty years as they provide insights into the nature of electron transfer, ET, processes. This has led to a deeper understanding of many complex, redox-based, biological processes, which includes photosynthesis. MV systems have also formed the basis of several forms of molecular devices. The prototype synthetic MV system is the Creutz-Taube ion, (CT-ion). This apparently simple species illustrates the complexities of MV systems. Using a classification delineated by Robin and Day, it was first thought that the CT-ion was either a Class II (valence localized, electron hoping) or Class III (valence delocalized) system. However, after several decades of research, involving many groups and a wide range of experimental and computational techniques, Meyer and colleagues suggested that the CT-ion is a hybrid, valence localized/solvation sphere averaged Class II/III system.

As part of a program to develop novel systems for the recognition of anions, bio-anions, and biomolecules, the Thomas group has been investigating the self-assembly of oligonuclear metallomacrocycles, such as the trinuclear macrocyclic bowl $\mathbf{1}^{3+}$, Figure 1, assembled from Ru^{II}([9]aneS_3) fragments and 9-methyladenine, 9MA, bridging ligands. An understanding of the host-guest properties of this redox-active system requires insights from both of the research areas described above.

Although the macrocycle is isolated as a Ru^{II}_3 complex, it is oxidized to its Ru^{III}_3 state in three electrochemical steps, going through two separate – $[Ru^{II}_2Ru^{III}]$ and $[Ru^{II}Ru^{III}_2]$ – MV states. Surprisingly, due to the novel connectivity of metal centers and bridging ligands within the MV structures, it is a Class II system in the $[Ru^{II}_2Ru^{III}]$ state, but a Class III system in the $[Ru^{II}Ru^{III}_2]$ state. The host-guest properties of the macrocycle and their effect on its redox properties have been investigated. These studies revealed a unique phenomenon: without any concomitant change in potential, anions can be used to switch the assembly from one mixed valence state to another, a process that is driven by the host-guest chemistry of the macrocycle. These initial studies were carried out using halide anions - chosen because their simple spherical geometry allowed us to investigate the effect of size on guest binding and were compared to the host's interaction with the nonpolar tetrahedral ClO_4^- anion, which was found to be very weak.

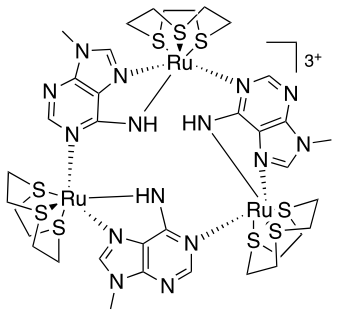

Figure 1. Structure of macrocycle $\mathbf{1}^{3+}$.

NMR studies revealed that $\mathbf{1}^{3+}$ binds halide ions in a 1:1 stoichiometry and displays good selectivity for intermediate sized guests: $>10^5$ M^{-1} for chloride, but <300 M^{-1} for fluoride. Although the metallomacrocycle has two possible binding pockets - an α pocket defined by the thiacrown ligands and the N-H binding sites from 9MA units, and a β pocket defined by 9MA bridging ligands projecting out to give an bowl shape aromatic surface – both the NMR studies and the crystal structure of [1]Br_3 indicated that the macrocycle binds halide guests exclusively in the α-binding pocket. Recognition of these anions entails a panoply of hydrogen bonds largely involving ethylenic C-H residues of the coordinated thiacrown ligands that define the lip of the pocket. However, the N-H moieties of the three 9MA bridging ligands form a tridentate "NH pincer" suited to binding larger anions and forming complementary hydrogen-bond to suitable accepting moieties. Hence, we sought to extend these studies and investigate the host-guest chemistry of $\mathbf{1}^{3+}$ with larger, structurally more complex, oxo-anions and compare the effect of these guests on the stability of the host's four redox states with the changes induced by halide ions.

Results and Discussion

NMR Studies

Previous studies had shown that the host binds nonpolar, more structurally complex, anions like perchlorate and hexafluorophosphate ions weakly in solution. As a result, we extended our studies to investigate more polar, potentially hydrogen bonding, oxo-anion guests. So that the effect of geometry, charge, and size could be explored, a mixture of tetrahedral ions and trigonal oxo-anions were chosen. We initially intended to extend these studies to dianions, however this was not possible as the host rapidly precipitated on the addition of guests such as SO_4^{2-}.

^{1}H-NMR titrations with the selected anions in d^3-MeCN all revealed distinctive changes in the spectra of the host – See SI. In particular, the NH protons of the 9MA bridging ligand showed downfield shifts that are characteristic of binding into the same cavity as halide ion guest. Furthermore, the intensity of these shifts was highly dependent on the nature of the guest. The largest shift, of 0.95 ppm, was observed for the CH_3COO^-, acetate ion, whilst the smallest (0.22 ppm) - induced by HSO_4^- - was almost comparable to that observed for perchlorate (0.12 ppm). In fact, the range of these values are less than those obtained for halide guests, which stretch from 3.65 ppm (F^-) to 0.52 ppm (I^-); however, a closer analysis of these data reveals that the two sp^2-based trigonal anions all produced larger shifts than the sp^3-based tetrahedral anions – Table 1.

Table 1. Anion guest induced ^{1}H-NMR shifts in the NH signals on 9MA bridging ligand of host $\mathbf{1}^{3+}$ and the K_a estimates for 1:1 anion binding derived from these data[a]

Anion	Δ δ/ppm	K_a/M^{-1}
CH_3COO^-	0.95	720
$(CH_3COO)_2^{2-}$	0.45	490
HSO_4^-	0.22	1200
NO_3^-	0.52	260
$H_2PO_4^-$	0.27	490
ClO_4^-	0.12	120

[a]To aid comparisons, data for ClO_4^- previously reported in ref xx is also included.

The oxo-anions also cause tell-tale shifts in the thiacrown-based signals, which further confirm they bind in the same site as halide ions. The interaction with the guest in this pocket has two effects on the thiacrown ligands. First, due to unfavorable steric interactions with the bound guest that increase the rigidity of the host, the overall conformational flexibility of the co-ordinated thiacrowns ligands will be reduced; an effect that is at its greatest for residues projecting into the interior of the binding pocket. Second, specific ethylene protons of the thiacrown ligands make hydrogen-bonding contacts to the anionic guest, and their resulting downfield shifts are dependent on the strength of their interaction with the guest. Generally speaking, compared to halides, the oxo-anion guests induce less profound changes in these signals – however they are still extensive – See SI.

Using the shifts in the NH protons of the 9MA bridging ligand, binding curves for the interaction with each guest were constructed. The constructed curves initially show saturation binding interactions, as confirmed by Job plots – Figure 2A.

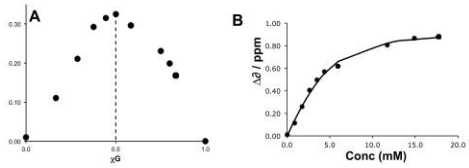

Figure 2. **A** – ^{1}H-NMR-based Job plot for the interaction of $\mathbf{1}^{3+}$ with the acetate anion in d^3-MeCN. **B**. ^{1}H-NMR-based titration with the same anion using shifts in NH protons of the 9MA. The continuous line is a fit to a 1:1 binding isotherm.

For these ions, fits to a 1:1 binding model using the shifts in the bridging ligand NMR signals were carried out, Figure 2B. The estimated association binding constant, K_a, values are summarized in Table 1.

As for our previous studies on halides, there is not a direct correlation between the magnitude of signal shifts – which actually reflect polarization – and the binding affinities. For the structurally complex anions studied herein, the binding affinity for hydrogen sulfate is highest. Despite having a lower charge density than halide anions, the overall affinity for this anion is comparable to those reported for some of the halides and, while affinities for the other oxo species are lower, they are similar in magnitude to the value reported for the interaction

Commented [JRBG1]: Maybe we can add a Figure similar to Figure 12 but without the anion (anion is replaced with the label alpha or beta) to the SI for better showing what is being described here.

Alternatively, the Figure can be similar to Figure 5A but with the anions replaced with the labels alpha / beta.

with fluoride guest, the halide with the lowest binding affinity (283 M^{-1}). The trend in affinities does not simply map onto the size of the guest but loosely correlates with the Lewis base strengths of the anions, indicating that hydrogen bond interactions are involved in the recognition process. Taken with the pattern of observed NMR shifts, these data are consistent with binding to the same receptor site involved in halide guest recognition.

Electrochemical Studies

Due to anion-induced precipitation at the concentrations required for cyclic voltammetry studies, titrations with only three of the oxo-anion guests – namely the acetate, nitrate, and perchlorate ions – were possible. However, these three guests do span a good range of oxo-anion binding affinities for the isovalent Ru^{II} macrocycle, thus providing insights into the effect of the anions on the host's electrochemical response.

Table 2. Maximum electrochemical shifts (mV) for [**1**]$(PF_6)_3$ induced by addition of oxo anions.[a]

Anion	$\Delta E_p(1)$	$\Delta E_p(2)$	$\Delta E_p(3)$
ClO_4^-	-10	-10	-35
NO_3^-	-50	-70	-45
CH_3COO^-	-15	-115	0

[a]In these conditions, the three oxidations of [**1**]$(PF_6)_3$ on its own were observed at 0.775 V, 0.910 V, and 1.270 V, respectively.

Unlike previous electrochemical studies involving halide ions that were complicated by the redox activity of the guests, on addition of oxo-anion, shifts in the three redox couples of host **1** are straightforwardly detected using square wave voltammetry. Each oxidation process of the host displays shifts that are characteristic of the individual guest employed – Table 2.

In a previous study we pointed out that the $\mathbf{1}^{3+}$ – $\mathbf{1}^{6+}$ redox chain is somewhat similar to a dynamic combinatorial library of host architectures in which host-guest interactions select for, and stabilize, the "best" host redox state. To investigate this issue in more details, binding affinities for guests were estimated using methods first developed for redox active crown and cryptand hosts.

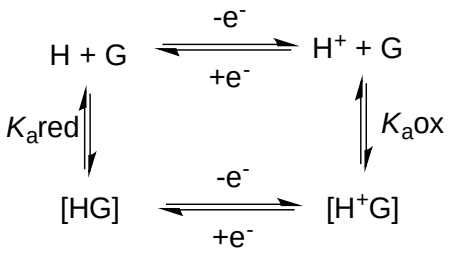

Scheme 1. Electrochemical and chemical equilibria for the interaction between an electroactive host and a non-electroactive guest.

For any redox active host, a thermodynamic cycle – as shown in Scheme 1 – involving the electrochemical potentials of the free and bound host (E_H and E_{HG} respectively) and the binding affinity of the individual oxidations states ($K_a$red and $K_a$ox respectively) can be constructed. This cycle leads to the relationship:

$$K_a\text{red}/K_a\text{ox} = \exp[-(F/RT)(E_H - E_{HG})]$$

Therefore, given the NMR-derived stoichiometry and binding affinities of $\mathbf{1}^{3+}$ and the electrochemical shifts for generation of $\mathbf{1}^{4+}$ in the absence and presence of specific guests, $K_a(\mathbf{1}^{4+})$ values can be estimated through this relationship.

Once values for $K_a(\mathbf{1}^{4+})$ are obtained, these figures along with the second oxidation potential in the presence and absence of the specific guest, can provide an estimate of $K_a(\mathbf{1}^{5+})$. Finally, this latter figure can be used with data for the third oxidation processes to estimate $K_a(\mathbf{1}^{6+})$. The analyses of the data collected in this study and in our previous study involving halide ions are summarized in Table 3.

Table 3. Estimated binding affinities for anions at the metallomacrocyclic host in different oxidation states.[a]

Guest	$K_a(\mathbf{1}^{3+})$	$K_a(\mathbf{1}^{4+})$	$K_a(\mathbf{1}^{5+})$	$K_a(\mathbf{1}^{6+})$
ClO_4^-	120	177	261	1.02×10^3
NO_3^-	260	1.8×10^3	2.8×10^4	1.6×10^5
CH_3COO^-	720	1.3×10^3	1.1×10^5	1.1×10^5
F^-	285	1.4×10^4	1.5×10^6	1.1×10^8
Cl^-	1.6×10^5	1.7×10^7	1.5×10^9	3.3×10^9
Br^-	3.9×10^4	4.9×10^5	2.4×10^6	1.6×10^6

[a]Binding affinities for the three halide anions were calculated using the electrochemical data obtained in ref XX.

The results reveal that across the four oxidations states anion- binding affinities span seven orders of magnitudes, with selectivity towards halides being particularly apparent. A graphical comparison of these data reveals some interesting effects – Figure 3. For example, affinities for the smallest anion, fluoride, show the simplest trend; K_a for F^- increases by two orders of magnitude for each increase in positive charge on the host, suggesting that increases in electrostatic interactions makes the largest contribution to enhanced binding. However, more complex trends are observed with other guests.

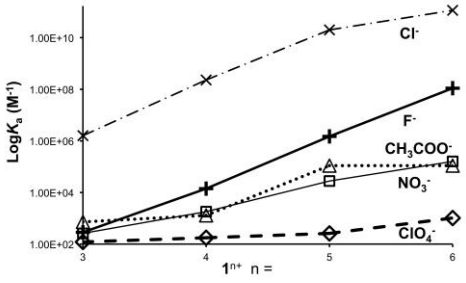

Figure 3. Trends in estimated K_a values for the four different oxidation states of self-assembled host $\mathbf{1}^n$.

Although $\mathbf{1}^{6+}$ binds chloride with picomolar affinity – figures that are comparable with some of the highest values for anion-binding receptors – the interaction is still slightly lower than expected by the simple linear trend observed for $\mathbf{1}^{3+}$ – $\mathbf{1}^{5+}$ with chloride. More strikingly, although acetate is bound with the

third highest affinity by all the redox states of the host, estimates of $K_a(CH_3COO^-)$ for $\mathbf{1}^{6+}$ are *identical* to $\mathbf{1}^{5+}$, confirming that the interaction of this host with larger and more complex anions is not simply driven by electrostatics. Indeed, there is an increased electrostatic contribution to binding in $\mathbf{1}^{6+}$ compared to $\mathbf{1}^{5+}$ and yet they bind acetate with the same affinity. These observations insinuate that more specific host-guest interactions with this guest are optimized in the $\mathbf{1}^{5+}$ redox state. Further evidence for this hypothesis is provided by the relative stability of individual MV states in the presence of specific guests.

Table 4. Comproportionation constants[a] for $\mathbf{1}^{4+}$ and $\mathbf{1}^{5+}$ in the presence of various anions.[b]

Guest	ΔEp(2,1)/mV	$K_c(\mathbf{1}^{4+})$	ΔEp(3,2)/mV	$K_c(\mathbf{1}^{5+})$
PF_6^-	135	195	360	1.3×10^6
ClO_4^-	135	195	335	4.7×10^5
NO_3^-	115	90	385	3.4×10^6
CH_3COO^-	35	4	475	1.1×10^8
F^-	85	28	380	2.8×10^6
Cl^-	140	236	430	2.0×10^7

[a]Calculated using the expression $\log K_c = [\Delta E/0.059]$. [b]To aid comparisons, values for F^- and Cl^- were re-assessed in identical conditions.

The shifts in potential induced by individual guest anions change the "electrochemical windows" in which each MV state of the bowl are accessed. The comproportionation constants, K_c, for each mixed valence state can be calculated through established relationships –Table 4, Figure 4.

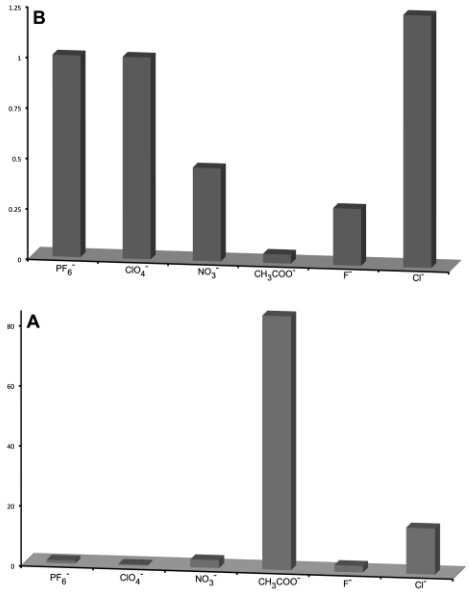

Figure 4. Proportional change in comproportionation constants for specific anions normalized for PF_6^- (A) values for $\mathbf{1}^{4+}$ (B) values for $\mathbf{1}^{5+}$.

Compared to the values for the original PF_6^- salt, these figures show that ClO_4^- has little effect on K_c values of the two MV states. This is unsurprising as both systems are classically, relatively nonpolar, non-coordinating ligands. However, other anions induce large changes in these constants.

The changes in K_c induced by nitrate ions and fluoride are somewhat similar: both anions destabilize the $\mathbf{1}^{4+}$ state but slightly stabilize the $\mathbf{1}^{5+}$ state. Chloride and acetate guests induce more distinctive changes in K_c values. Chloride anion is the only guest that increases the K_c of $\mathbf{1}^{4+}$ compared to PF_6^-, although the stabilization effect (×1.25) is relatively small compared to the >×15 observed for the $\mathbf{1}^{5+}$ state. Even more strikingly, acetate destabilizes the $\mathbf{1}^{4+}$ state, with $K_c(\mathbf{1}^{4+})$ being only 0.045 of the $K_c(PF_6^-)$ value. As a consequence, $K_c(CH_3COO^-)$ is reduced to a statistical value of 4, observed in non-interacting systems. Contrastingly, acetate greatly stabilizes the $\mathbf{1}^{5+}$ state leading to a $K_c(\mathbf{1}^{5+})$ that is enhanced by almost two orders of magnitude. This distinctive pattern of preferential stabilization offers further evidence that, compared to the host's three other accessible oxidation states, $\mathbf{1}^{5+}$ has an exceptionally strong interaction with acetate.

Crystallography Studies

To investigate the solid-state host properties of $\mathbf{1}^{3+}$ with structurally more complex anions, attempts were made to grow crystals of the host in the presence of a range of oxo-anions but these were not successful. However, X-ray quality crystals of its hexafluorophosphate salt were obtained, which led to somewhat unexpected results.

Surprisingly, the structure reveals that two anions make close contact with the macrocyclic cation – Figure 5A. Consistent with previous NMR studies, one anion is bound into the thiacrown-based α-face of the host, where an array of close contacts are made by hydrogen bond donor sites on the thiacrown and the N-H groups of the 9MA bridging ligands to fluorine atoms on the anion. However, a second anion sits at the open β-face of the bowl making close contacts with hydrogens on the 9-methyl groups of the 9MA bridging ligands, confirming that – in the solid phase at least - this face can also be a host site for larger and/or more lipophilic anions. This observation also insinuates that anion-π interactions may play a part in the host-guest interactions of the macrocycle.

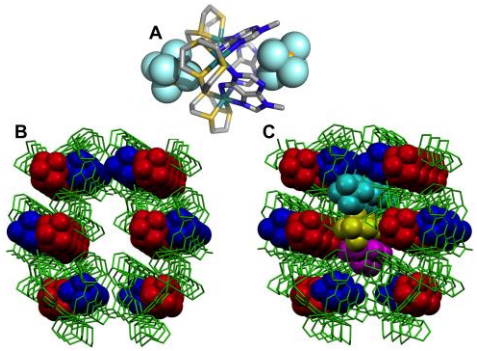

Figure 5. **A** – Interaction between the metallomacrocyclic cation and two hexafluorophosphate anions observed in the crystal structure of $[\mathbf{1}](PF_6)_3$. **B** Hexagonal channels defined by the

Commented [JRBG4]: 1.21, right?
Please check all the numbers

Commented [JRBG5]: This is true if the values in the Table are rounded. Otherwise, the increase is 14.7 times, which is less than 15. Maybe we can use ~ (approximately) instead of >

Commented [JRBG2]: Check whether the values for PF6- and ClO4- in columns 2 and 3 are exactly the same

Commented [JRBG6]: 0.021?

Commented [JRBG3]: The caption needs improvements.

Also, change the B in the top panel to A and change the A in the bottom panel to B.

interaction between the host and anions. **C** Hexagonal channels filled with the remaining hexafluorophosphate anions.

Unlike the previously reported structure with bromide anions, in which face-to-face macrocycles define a dimeric capsule, the interactions between the individual host cations and the two PF_6^- anions define hexagonal channels – Figure 5B, which are occupied by the remaining hexafluorophosphate anions – Figure 5C.

The NMR binding data in MeCN and the crystallographic structure imply that anion binding by the macrocycle in its different oxidation states is not simply driven by a step-wise increase in electrostatic interactions between host and guest. This is consistent with previous studies indicating that anionic guest recognition by macrocyclic hosts is not primarily driven by electrostatics in higher dielectric solvents like MeCN, but increasingly involves induction and dispersion forces. In our previous report we described initial computational studies that provided considerable insights into the interaction of $\mathbf{1}^{3+}$ with simple spherical halide anions. To investigate the issues described above in more detail, the interaction of each oxidation state of the macrocycle with oxo-anions were studied using computational methods. This work was further motivated by the fact that computational studies on the energetics of anion binding by macrocycles are still quite rare. Indeed, as far as we are aware, this is the first such study on the anion binding properties of a self-assembled metallomacrocycles host for anion guests or any multi-redox state receptor.

Computational studies

To obtain further insights into the host properties of **1**, in its different MV states, Gaussian09[1] was used to perform extensive DFT calculations within a polarized continuous solvent model (IEFPCM)[2] of acetonitrile, using the CAM-B3LYP functional with Grimme's D3 dispersion correction,[3] coupled with the LANL2TZ(f) basis set[4] for ruthenium and with the 6-31+G(d) basis set for the remaining elements. Moreover, for the higher oxidation states two alternative spin multiplicities were considered, 1 and 3 for $\mathbf{1}^{5+}$ and 2 and 4 for $\mathbf{1}^{6+}$. Henceforth, these low- and high-spin species will be designated by *ls*-$\mathbf{1}^{5+}$and *ls*-$\mathbf{1}^{6+}$, and *hs*-$\mathbf{1}^{5+}$and *hs*-$\mathbf{1}^{6+}$, respectively. Further computational details are given in section X of the ESI.

In the optimized structure of free $\mathbf{1}^{3+}$ (see Figure S1), the computed Ru-S distances are equivalent and are indistinguishable between the three thiacrown ethers, with an average value of 2.360 ± 0.006 Å (Table S1). The Ru-N distances follow an identical pattern, independently of the coordination mode of the 9MA bridging ligands, with an average value of 2.152 ± 0.007 Å. In addition, while the Ru-N distances are identical to those observed in the single crystal X-ray structure of $\mathbf{1}^{3+}\cdot PF_6^-$, the computed Ru-S distances are *ca.* 0.07 Å slightly longer. Along the subsequent oxidation states, the Ru-S distances successively increase 0.015 ($\mathbf{1}^{4+}$), 0.013 ($\mathbf{1}^{5+}$) and 0.011 Å ($\mathbf{1}^{6+}$), with an average value of 2.398 ± 0.019 Å for the later oxidation state. On the other hand, the Ru-N average distances also slightly change, decreasing from $\mathbf{1}^{3+}$ (2.152 ± 0.007 Å) to $\mathbf{1}^{6+}$ (2.104 ± 0.061 Å). In addition, the Ru-S and Ru-N distances are independent of the spin multiplicities in the $\mathbf{1}^{5+}$ and $\mathbf{1}^{6+}$ hosts (Table S1).

The energy difference between *ls*-$\mathbf{1}^{6+}$ and *hs*-$\mathbf{1}^{6+}$ is only 0.835 kcal mol^{-1}, while *ls*-$\mathbf{1}^{5+}$ and *hs*-$\mathbf{1}^{5+}$are almost degenerate (see Table S2), indicating that both spin multiplicities for these oxidation states are likely.

The analysis of the Mulliken spin densities (Table 5) for free $\mathbf{1}^{n+}$ MV states reveals that in $[Ru^{II}_2Ru^{III}]$ state ($\mathbf{1}^{4+}$) exists a single unpaired electron. For the subsequent $[Ru^{II}Ru^{III}_2]$ MV state ($\mathbf{1}^{5+}$), in the diamagnetic low-spin configuration, the spin densities show that the unpaired electrons of the two Ru^{III} centers have opposite spins, consistent with their coupling through the 9MA bridges, while in the high-spin state, naturally, no coupling is observed. In $\mathbf{1}^{6+}$ $[Ru^{III}_3]$ host, the spin densities indicate that the odd electrons in two Ru^{III} centers have opposite spins in *ls*-$\mathbf{1}^{6+}$, while in *hs*-$\mathbf{1}^{6+}$ the three electrons of the Ru^{III} centers have the same spin.

Table 5. Mulliken spin densities on Ru centers in free $\mathbf{1}^{n+}$ (n= 4, 5 or 6), with the corresponding electron configurations.

Oxidation state	Mulliken spin densities (a.u.)	Electron configuration
$\mathbf{1}^{4+}$	+0.001 ; +0.001 ; +0.685	↑↓ ; ↑↓ ; ↑
ls-$\mathbf{1}^{5+}$	-0.001 ; +0.784 ; -0.649	↑↓ ; ↑ ; ↓
hs-$\mathbf{1}^{5+}$	+0.011 ; +0.777 ; +0.628	↑↓ ; ↑ ; ↑
ls-$\mathbf{1}^{6+}$	+0.788 ; +0.755 ; -0.773	↑ ; ↑ ; ↓
hs-$\mathbf{1}^{6+}$	+0.781 ; +0.771 ; +0.774	↑ ; ↑ ; ↑

The anion binding properties of **1** were initially ascertained from the electrostatic potential distribution mapped onto the electron density surface (V_S) calculated with Multiwfn[5-6] for the four oxidation states. Overall, the most positive region of V_S covers the [9]aneS$_3$ ligands and the three N-H binding units of the 9MA bridges of the α pocket, while the less positive region naturally encloses the aromatic moieties of the 9MA bridging ligands of the β pocket, as illustrated in Figure S2. The highest value of V_S ($V_{S,max}$, see Table S3) is found inside the α pocket, near the three N–H binding units, and grows linearly with the oxidation state (R^2 = 0.999, Figure S3). The β pocket also displays well defined electrostatic potential regions enclosing high V_S points (Table S3) that follow the same order of $V_{S,max}$ (R^2 = 0.998, Figure S3). Noteworthy, the difference between the α and β highest V_S values decreases throughout the oxidation states (Table S3), suggesting the possibility of anion binding in the β pocket at least at the higher oxidation states of the host, as demonstrated below.

Having ascertained the main structural and electronic features of **1** relevant for anion recognition, the DFT calculations were extended to its anion associations. In agreement with the experimental binding data and first theoretical insights, CH_3COO^-, NO_3^-, ClO_4^-, HSO_4^-, $H_2PO_4^-$, and PF_6^- were positioned in the room provided by the α pocket or, alternatively, by the β pocket, with the host in the four different oxidation states and spin multiplicities. Moreover, for acetate hosted in the β pocket, the anion was positioned with either the carboxylate or methyl groups pointing inwards the cavity, thus a total of 78 putative binding arrangements were generated and investigated. The optimized structures of $\mathbf{1}^{n+}$ with oxo-anions encapsulated in these two alternative binding scenarios are shown in Figures S4-S14. Overall, the energy differences observed between the low-

Commented [JRBG7]: Font size is 0.5 pts bigger than that used in the previous section.

Commented [JRBG8]: To be compatible with the labeling in page 1 (right column)

Commented [JRBG9]: Only 66 arrangement are shown in Figures S4-S14. This suggests that we are only showing the most stable ones for acetate, right?
We may want to add the words "most stable" somewhere around here.

and high-spin $\mathbf{1}^{5+}$ and $\mathbf{1}^{6+}$ free hosts are maintained in their anion associations (see Table S2), with the low-spin $\mathbf{1}^{5+}$ and $\mathbf{1}^{6+}$ being slightly favoured. In agreement, unless otherwise stated, in the subsequent structural and energetic analyses the $\mathbf{1}^{5+}$ and $\mathbf{1}^{6+}$ complexes are discussed independently of their alternative electronic configurations. Furthermore, the Mulliken spin densities observed in the free hosts are not perturbed by the anion binding (see Table S4).

Energetic insights into the host-guest associations were obtained estimating the binding interaction energies between $\mathbf{1}^{n+}$ hosts and the anionic guests (ΔE_{HG}), as:

$$\Delta E_{\mathrm{HG}} = E_{\mathrm{HG}} - (E_{\mathrm{H}} + E_{\mathrm{G}})$$

where E_{HG}, E_{H} and E_{G} correspond to the DFT IEFPCM ground state energies for the optimized structures of the host-anion association (HG), the host (H), and the oxo-anion guest (G), respectively, including the zero-point energy corrections. Overall, the ΔE_{HG} values gathered in Table S5 indicate that interactions between the $\mathbf{1}^{n+}$ hosts and the guest anions are stronger in the α pocket than in the β one, i.e., the oxo-anions are preferentially hosted in the former, in line with the ^{1}H-NMR anion binding data (*vide supra*) for $\mathbf{1}^{3+}$., with the energy differences between the alpha and beta oxo-anions hosted systems ranging from -15.98 (*hs*-$\mathbf{1}^{6+}$·CH_3COO^-) to -4.50 kcal mol^{-1} (*hs*-$\mathbf{1}^{5+}$·ClO_4^-). Moreover, regardless of the host binding cavity, the absolute values of ΔE_{HG} for each oxo-anion linearly increase with the host's oxidation state (see Figure 6). On the other hand, in the α pocket, the ΔE_{HG} values show that the binding affinity order is not preserved along the host's oxidation states, changing from $\mathbf{1}^{3+}$ ($H_2PO_4^-$ > HSO_4^- > CH_3COO^- ≈ ClO_4^- > NO_3^-),[7] to $\mathbf{1}^{4+}$ ($H_2PO_4^-$ > CH_3COO^- ≈ HSO_4^- > ClO_4^- ≈ NO_3^-), and then to $\mathbf{1}^{5+}$ ($H_2PO_4^-$ > CH_3COO^- > HSO_4^- > NO_3^- > ClO_4^-),being maintained in $\mathbf{1}^{6+}$. In all oxidation states there is a preference for $H_2PO_4^-$, which is inconsistent with the experimental binding data. These energetic trends are also obtained from the binding enthalpies as well as from the corresponding binding free energies, both estimated using the DFT optimized structures (see the detailed energetic analysis summarized in Table S6).

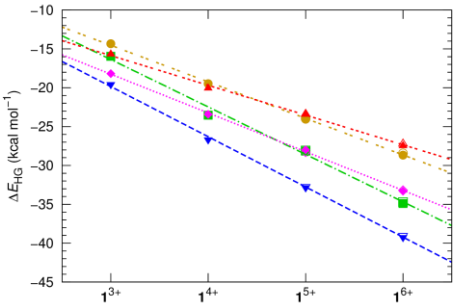

Figure 6. Variation of the ΔE_{HG} (kcal mol^{-1}) between $\mathbf{1}^{n+}$ and the oxo-anions in the DFT optimized structures of their associations, together with the corresponding linear fits ($R^2 \geq 0.99$). Key: CH_3COO^- (■), NO_3^- (●), ClO_4^- (▲), HSO_4^- (◆) or $H_2PO_4^-$ (▼). The high-spin electron configurations are represented by the open points (□, ○, △, ◇ and ▽).

Having established that the oxo-anions are preferentially recognized in the α pocket, only these optimized binding scenarios will be thoroughly analysed. Regardless of the size and binding geometry of the oxo-anions, one oxygen atom is entirely embedded into the α pocket and bonded through three convergent hydrogen bonds from the three N-H binding sites of $\mathbf{1}^{n+}$, as illustrated in Figure 7 for the $\mathbf{1}^{3+}$ host-guest systems. Moreover, the computed structures also display multiple C–H···O close contacts between the non-coordinated oxygen atoms and C–H groups from the thiacrown ethers as indicated by ^{1}H NMR spectra of $\mathbf{1}^{3+}$ upon addition of the oxo-anions.

The average dimensions computed for the three N–H···O hydrogen bonds are summarised in Table S7, while the distance from the anion's central atom (A_c = S, P, N, Cl or C_{COO} in HSO_4^-, $H_2PO_4^-$, NO_3^-, ClO_4^- or CH_3COO^-, respectively) to the N_3 plane, determined by the three N atoms from the N–H groups of the 9MA bridging ligands, are reported in Table S8. The A_c···N_3 distances decrease with the increment of the host's positive charge, with the anions being progressively buried deeper in the α pocket, as a result of the charge-assisted hydrogen bonding interactions (*vide infra*). For instance, for the basic acetate, the A_c···N_3 distances go from 3.616 ($\mathbf{1}^{3+}$) to 3.387/3.382 Å (*ls*-$\mathbf{1}^{6+}$/*hs*-$\mathbf{1}^{6+}$), while for the remaining oxo-anions the variation is less than 0.2 Å. The host charges also affect the hydrogen bonding dimensions, with a concomitant slight drop of the N···O distances between incremental oxidation states, with the differences between the $\mathbf{1}^{3+}$ and $\mathbf{1}^{6+}$ of *ca*. 0.14 Å.

In spite of the anion guests' preference for the α pocket, as reported above, the V_S in the β pocket should facilitate the recognition of the oxo-anions through anion-pi interactions. Accordingly, for both low- and high-spin $\mathbf{1}^{6+}$·CH_3COO^- complexes, the binding arrangement with the anion's oxygen atom pointing towards the highest V_S in the β pocket (Figure S6) is favoured by *ca*. 3.9 kcal mol^{-1}, while the anion disposition with the methyl group pointing towards the inner faces of the electron deficient 9MA bridging ligands (Figure S5) is preferred by *ca*. 5.6, 3.2, and 1.5 kcal mol^{-1} in the $\mathbf{1}^{3+}$, $\mathbf{1}^{4+}$ and $\mathbf{1}^{5+}$ complexes, respectively. Moreover, in the later spatial disposition (methyl group facing a 9MA), the position of the acetate anion is nearly independent of the host's oxidation state, with A_c···N_3 distances *ca*. 4.0 Å, while in the alternative disposition this structural parameter decreases from 5.575 ($\mathbf{1}^{3+}$) to 4.062/4.060 Å (*ls*-$\mathbf{1}^{6+}$/*hs*-$\mathbf{1}^{6+}$), as consequence of the growing electrostatic interactions and dispersion forces between the negatively charged carboxylate group and the electron deficient 9MA bridging ligands. This structural trend is also observed for the remaining anions when they were putatively hosted in the β pocket (see Table S9).

Commented [JRBG12]: Symbols for ClO4- and H2PO4- in the caption look as red and blue rectangles, which differs from the symbols displayed in the graph. Please check whether this is a problem originated by different versions of the MS Word or anything else.

Commented [JRBG13]: Here, they look correct. However, it is not easy to find them in the Figure because they are overlapping other symbols.
I think we should alert the reader for the overlapped symbols

Commented [JRBG10]: Too decimals is enough

Commented [JRBG11]: What are we presenting here, differential enthalpies at 0 K, i.e., values obtained from total energies + zero-point vibrational energies, differential enthalpies at 298.15 K, i.e., values obtained from total energies + zero-point vibrational energies + other thermal corrections?
From the text above, I am assuming the former case.
Gibbs energies are at T = 298.15 K, right?
This has to be clarified.

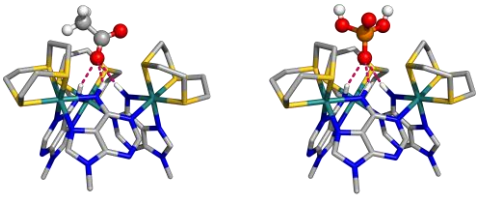

1^{3+}-CH_3COO^- 1^{3+}-$H_2PO_4^-$

Figure 7. DFT optimised structures of $\mathbf{1}^{3+}$ associations with CH_3COO^- and $H_2PO_4^-$. The N–H···O hydrogen bonds are drawn as pink dashed lines. The hosts' C–H hydrogen atoms were hidden for clarity.

To evaluate the conformational distortion derived from the anion binding, the root-mean-square deviations (RMSD) were calculated between free $\mathbf{1}^{n+}$ and $\mathbf{1}^{n+}$ associated with each anion excluding the H atoms. The values, summarised in Table S10, ranging from 0.077 to 0.183 Å, indicate that the $\mathbf{1}^{n+}$ hosts have enough room in the α pocket to accommodate these anions, regardless of their shape, without a significant distortion of the flexible thiacrown units. Hosting the anions in the β pocket, with RMSD values between 0.047 and 0.176 Å, suggests a similar degree of distortion.

Thus far, our analysis has shown that the oxo-anion recognition undoubtedly occurs in the α pocket, via hydrogen bond interactions. However, due to the puzzling ΔE_{HG} values, we decided to ascertain the strength of the hydrogen bonding interactions between the host in $\mathbf{1}^{3+}$, $\mathbf{1}^{4+}$, $\mathbf{1}^{5+}$ and $\mathbf{1}^{6+}$ and each oxo-anion guest through the Quantum Theory of Atoms in Molecules (QTAIM),[8,5] and by Natural Bond Orbital (NBO) analysis.[9-10]

Following the structural analysis, the QTAIM evaluation shows the existence of a bond critical point (BCP) between every N–H binding site and the anion's oxygen atoms involved in the three hydrogen bond interactions, as illustrated in Figure S15 for CH_3COO^- or $H_2PO_4^-$ hosted in the α-binding pocket of $\mathbf{1}^{3+}$. The electron density (ρ), its Laplacian derivative ($\nabla^2\rho$) and the potential energy density ($\mathcal{V}$), all averaged from the calculated data at the three BCPs, are gathered in Table S11, together with the energy of the hydrogen bonds (E_{HB}), estimated from $\mathcal{V}$ as $E_{HB} = ½\mathcal{V}$.[11] The $\nabla^2\rho$ values are positive for all host-guest systems, indicating a depletion of the electron distribution consistent with the formation of the hydrogen bonding interactions. Moreover, the E_{HB} values for each hosted anion yields good linear relationships with the host's oxidation states (see Figure 8), indicating that the hydrogen bonds strength increases with the host net charge. On the other hand, for each oxidation state of the host, the average E_{HB} values along the oxo-anion's series (see Table S7) follow the same order CH_3COO^- > $H_2PO_4^-$ > NO_3^- > HSO_4^- > ClO_4^-, indicating that the N–H···O hydrogen bonding interactions with the more basic acetate are the strongest ones, while the tetrahedral perchlorate is the weakest bonded anion. Moreover, for $\mathbf{1}^{3+}$, this hydrogen bond strength trend is consistent with the ^{1}H-NMR binding data (see Table 1), apart from HSO_4^-, with the highest association constant. On the other hand, for the anion complexes of $\mathbf{1}^{5+}$and $\mathbf{1}^{6+}$, the E_{HB} values seem to be nearly independent of the spin multiplicities.

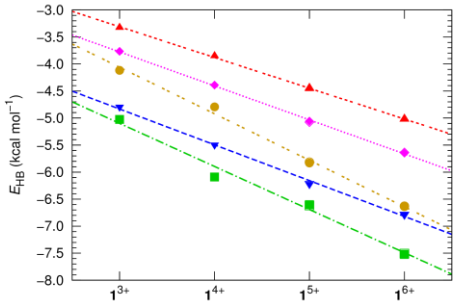

Figure 8. Average E_{HB} energy values (kcal mol^{-1}) for the hydrogen bonds between $\mathbf{1}^{n+}$ and CH_3COO^- (■), NO_3^- (●), ClO_4^- (▲), HSO_4^- (♦) or $H_2PO_4^-$ (▼) as a function of $\mathbf{1}^{n+}$ oxidation state, together with their linear fits ($R^2 \geq 0.95$). The high-spin electron configurations are represented by the open points (□, ○, △, ◇ and ▽).

In the NBO analysis, the three N–H···O hydrogen bonds were evaluated as interactions between the electron lone pairs of an oxygen atom of the oxo-anion and the N–H antibonding orbitals of $\mathbf{1}^{n+}$: $n_O \rightarrow \sigma^*_{NH}$. The interaction between every anion and $\mathbf{1}^{n+}$ hosts, leads to a decrease of the occupancy of the anions' lone pair orbitals in the complex relatively to the free anion, while the occupancy of the N–H antibonding orbitals of the hosts increases relatively to the corresponding free $\mathbf{1}^{n+}$. The difference between the orbitals' occupancy of the free and hosted anion change linearly with the host oxidation state as shown in **Figure 9**. Concomitantly, the difference between the orbitals' occupancy in the free and in the anion associated to $\mathbf{1}^{n+}$ follows a reverse linear order. Overall, the natural population analysis (NPA), indicates that the anion binding is accompanied by a charge transfer from the anion to the host (see Figure S16). In other words, the anion binding occurs with a progressive accumulation of electron density between the N–H binding sites and the hydrogen bonded anion oxygen atom, spanning across the host oxidation states, as illustrated in **Figure 10** with the electron density difference maps for $\mathbf{1}^{n+}$ associated with HSO_4^- (see ESI for details).

Commented [JRBG14]: Same problem as in Figure 6 detected here with the symbols of ClO4- and H2PO4-

Commented [JRBG15]: As above, we should alert the reader for the overlapped symbols

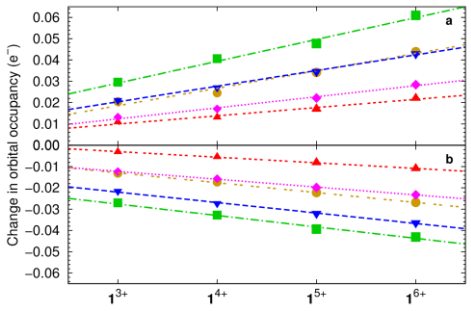

Figure 9. Change in orbital occupancy (e^-) as a function of $\mathbf{1}^{n+}$ oxidation state (all data have linear fits with $R^2 \geq 0.96$). **a** – difference between the sum of the three σ^*_{NH} orbitals in free $\mathbf{1}^{n+}$ and in their anion associations; **b** – difference between the n_O orbital in the free oxo-anions and in the respective host-guest associations. Key: CH_3COO^- (■), NO_3^- (●), ClO_4^- (▲), HSO_4^- (◆) or $H_2PO_4^-$ (▼). The high-spin electron configurations are represented by the open points (□, ○, △, ◇ and ▽).

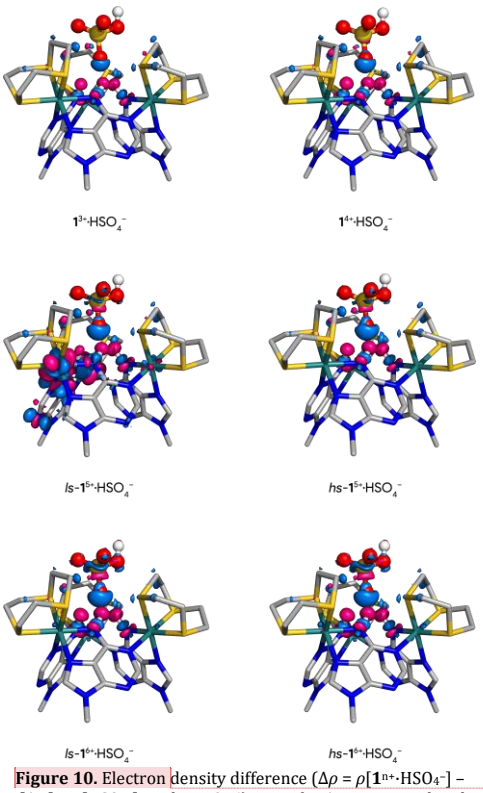

Figure 10. Electron density difference ($\Delta\rho = \rho[\mathbf{1}^{n+}\cdot HSO_4^-] - \rho[\mathbf{1}^{n+}] - \rho[HSO_4^-]$, with n = 3–6) maps for $\mathbf{1}^{n+}$·associated with HSO_4^-. Blue indicates increase of electron density (+0.002 $e a_0^{-3}$ contour) and magenta indicates loss of electron density (–0.002 $e a_0^{-3}$ contour).

The donor-acceptor stabilization energies (E^2) estimated by the 2nd-order perturbation theory for the three N–H···O hydrogen bonds between each oxo-anion and $\mathbf{1}^{n+}$ (see Table S12), also reveal that these synergetic interactions are also largely dependent of the host oxidation state, mirroring the linear tendency previously obtained with the $\mathcal{V}$ values in BCPs (see Figure S17).

In summary, the three quantum descriptors, ΔE_{HG}, E_{HB}, and E^2 show that the binding affinity of $\mathbf{1}^{n+}$ towards the oxo-anions is mainly dictated by the N–H···O charge-assisted hydrogen bonding interactions. In line, when the logarithms of the association constants (Table 3) estimated for tetragonal (ClO_4^-) and trigonal (NO_3^-) anions are plotted against the absolute values of E_{HG}, E_{HB}, or E^2 highly linear relationships are observed (Figure 11, $R^2 \geq 0.87$).

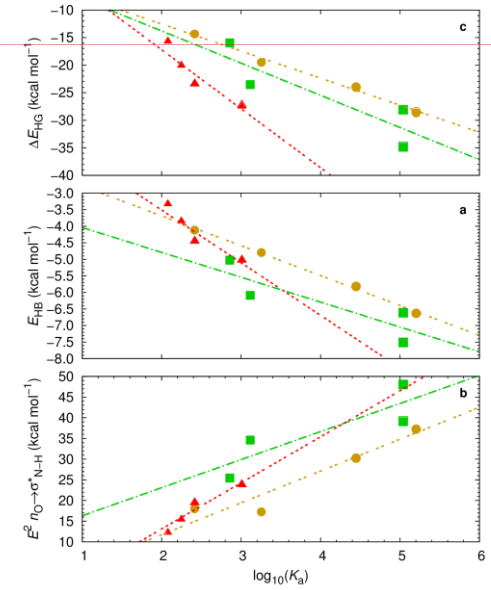

Figure 11. Quantum parameters as a function of $\log_{10}(K_a)$ for the anion associations of $\mathbf{1}^{n+}$ and CH_3COO^- (■), NO_3^- (●), ClO_4^- (▲), together with the corresponding linear fits: **a** Variation of the ΔE_{HG} (kcal mol^{-1}) between $\mathbf{1}^{n+}$ and the oxo-anion ($R^2 \geq 0.75$); **b** Average E_{HB} energy values (kcal mol^{-1}) for the hydrogen bonds between $\mathbf{1}^{n+}$ and the oxo-anion ($R^2 \geq 0.72$); **c** Variation of the 2nd-order perturbation stabilisation energies of $n_O \rightarrow \sigma^*_{N-H}$ (kcal mol^{-1}) for the N–H···O interactions ($R^2 \geq 0.70$).

The analysis of the highest-energy occupied molecular orbitals (HOMO) between the free and anion associated **1** host, in its four different oxidation states, reveals that the main contribution for this frontier molecular orbital is from

Commented [JRBG16]: As above, same problem with the symbols

Commented [JRBG18]: Problem with the symbol for ClO4-

Commented [JRBG19]: The labels of the panels c, a and b (see the top-right corner) must be a, b and c, respectively.

Commented [JRBG17]: This Figure can be moved to the ESI

the three 9MA bridging ligands, even in the anion associations (see Figure S18). The HOMO energy values, given in Table S13, as expected, lower with the increasing host's oxidation state. On the other hand, the presence of the anions in the α pocket only slightly raises the energy of the HOMO in all oxidation states, in agreement with their negligible contributions for this orbital. The ionization potentials (IP) of 1^{n+}, both free and anion associated, were roughly estimated from the HOMO energies, using Koopman's theorem ($IP_K = -E_{HOMO}$),[12] as well as through the more accurate adiabatic approach,[13] using the differences between the ZPE corrected energies of the optimized structures in consecutive oxidation states ($IP_A = E^{(n+1)+} - E^{n+}$, with n ranging from 3 to 5). The IP_A values are gathered in Table S14 together with the IP_K ones. Overall, the former IP values indicate that the energy required to remove an electron increases with the oxidation state of $\mathbf{1}^{n+}$. Moreover, the hosted anions facilitate the successive oxidation of $\mathbf{1}^{3+}$, in agreement with the electrochemical data. Furthermore, in mirroring the ΔE_{HG} interaction energies, the tightly bonded $H_2PO_4^-$ is the anion that more easily enables the successive electron loss. The same theoretical oxidation insights can be found with the overestimated IP_K values.

The DFT computed structure of the $\mathbf{1}^{3+}{\cdot}PF_6^-$ complex (see Figure 12, left panel) has the octahedral anion lodged in the α pocket with the phosphorous atom only 4.05 Å away from the N_3 equatorial plane (*vide supra*), while in the X-ray crystal structure the anion is just outside the binding pocket, with a $A_c{\cdots}N_3$ distance of 4.50 Å. Three fluorine atoms establish three single N–H···F hydrogen bonds to $\mathbf{1}^{3+}$, with an average N···F distance of 3.14 ± 0.01 Å, being markedly shorter (*ca*. 0.5 Å) than those observed in the X-ray structure (see Table S14). On the other hand, in the β pocket (seeFigure 12, right panel), PF_6^- is also more deeply embedded in the computed structure than in the solid state one, with $A_c{\cdots}N_3$ distances of 5.128 and 5.986 Å, respectively (Table S14). Overall, these two binding arrangements are preserved along the remaining three oxidation states (see Figures S19 and S20), with the inherent shortening of the $A_c{\cdots}N_3$ distances and increase of the N–H···F hydrogen bonds' strength, as evident from the dimensions of these two structural parameters gathered in Table S15.

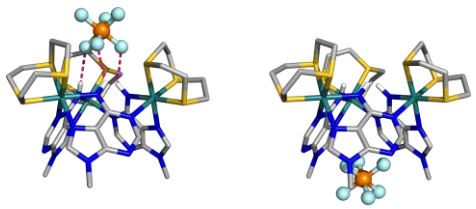

Figure 12. DFT optimized structures of $\mathbf{1}^{3+}$ associations with octahedral anion PF_6^- in the α or β pocket. The N–H···F hydrogen bonds are drawn as pink dashed lines. The C–H hydrogen atoms were hidden for clarity.

In agreement with its weak binding ability, the estimated ΔE_{HG}, E_{HB}, and E^2values for the PF_6^- interacting with α pocket of $\mathbf{1}^{n+}$ (summarised in Table S16) are lower when compared with those obtained for the oxo-anions, but follow equivalent energetic trends with the host's oxidation state (see Figure S21). On the other hand, in contrast with the clear preference of the oxo-anion for the α pocket of $\mathbf{1}^{n+}$, the $\Delta E_{HG\alpha\text{-}\beta}$ values for the PF_6^- systems show that its binding strength for the α pocket diminishes with the increase of the host's oxidation state (see Figure S22). Notably, in the last two oxidation states, independently of the spin multiplicities, the recognition of the octahedral anion is likely in either the α or β pocket, with the latter one being slightly favoured by *ca*. 0.3 and 0.6 kcal mol-1 in $\mathbf{1}^{5+}$ and $\mathbf{1}^{6+}$, respectively. The QTAIM analysis of the optimised β pocket associations of $\mathbf{1}^{n+}{\cdot}PF_6^-$ reveals that, as the $A_c{\cdots}N_3$ distance decreases (see Table S14), the number of BCPs between the fluorine atoms and the 9MA bridging faces of this bowl cavity increases, ranging from 9 to 12 for $\mathbf{1}^{3+}$ and $\mathbf{1}^{6+}$, respectively. In agreement, the total values of $\mathcal{V}$ decreased linearly with host's net charge, running almost parallel to $\mathcal{V}$ for the N–H···F hydrogen bonding interactions in the α pocket, as depicted in Figure S23. The E^2 values estimated for the PF_6^- hosted in the alternative binding pockets follow reverse linear trends when plotted against the host's oxidation states (see Figure S24). Moreover, the charge transfer from the octahedral anion to both binding cavities of $\mathbf{1}^{n+}$ was also evaluated, being more pronounced in the α pocket than in the β one (see Figure S25). In line, the ionisation energies (Table S17) indicate that PF_6^- does not facilitate the successive oxidation of $\mathbf{1}^{n+}$ to the same extension as the oxo-anions. Therefore, these findings seem to indicate that the progressive loss of the binding preference of PF_6^- across the four oxidation states for the α pocket is determined by the concomitant increase of electrostatic interactions and dispersion forces between PF_6^- and the π-electron-deficient 9MA bridging faces of the β pocket.

Conclusions

In agreement with the experimental data, the DFT calculations indicates that $\mathbf{1}^{n+}$, in its four oxidation states, hosts the oxo-anions into the α pocket through three synergetic hydrogen bonding interactions. The oxo-anion guests binding preference for the α pocket is independent of the oxidation state and spin multiplicity of this trinuclear macrocyclic receptor. In contrast, the theoretical energetic data indicate that the recognition of the octahedral PF_6^- anion in the $\mathbf{1}^{3+}$ and $\mathbf{1}^{4+}$ lower oxidation states mainly occurs in the α pocket, while the β pocket is preferred in the two subsequent oxidation states, due to the enhance of anion-π interactions.

The QTAIM and NBO analyses show that throughout the successive oxidation states of $\mathbf{1}^{n+}$, the strength of the charge assisted hydrogen bonds increases, leading to a progressive growth of the charge transfer from the oxo-anions to the metallo-macrocyclic host and its consequent stabilization.

ASSOCIATED CONTENT

(Word Style "TE_Supporting_Informati**on"). Supporting Information**. A brief statement in nonsentence format listing the

contents of material supplied as Supporting Information should be included, ending with "This material is available free of charge via the Internet at http://pubs.acs.org." For instructions on what should be included in the Supporting Information as well as how to prepare this material for publication, refer to the journal's Instructions for Authors.

AUTHOR INFORMATION

Corresponding Author

Email: james.thomas@sheffield.ac.uk; vitor.felix@ua.pt

Present Addresses

▲ Chemistry Department. Faculty of Science Misurata University, Misurata, Libya.

Author Contributions

The manuscript was written through contributions of all authors. / All authors have given approval to the final version of the manuscript.

Funding Sources

Any funds used to support the research of the manuscript should be placed here (per journal style).

Notes

Any additional relevant notes should be placed here.

ACKNOWLEDGMENT

V.F. is grateful for financial support from projects PTDC/QEQ-SUP/4283/2014 and CICECO – Aveiro Institute of Materials (UIDB/50011/2020 & UIDP/50011/2020), financed by National Funds through the FCT/MEC and co-financed by QREN-FEDER through COMPETE under the PT2020 Partnership Agreement. I.M. is grateful for a postdoctoral grant (BPD/UI98/6065/2018) under project "pAGE" (Centro-01-0145-FEDER-000003), co-funded by Centro 2020 programme, Portugal 2020, European Union, through the European Regional Development Fund. A.Z. is grateful to the Libyan government financial support through a PhD studentship.

REFERENCES

1. Frisch, M. J.; Trucks, G. W.; Schlegel, H. B.; Scuseria, G. E.; Robb, M. A.; Cheeseman, J. R.; Scalmani, G.; Barone, V.; Mennucci, B.; Petersson, G. A.; Nakatsuji, H.; Caricato, M.; Li, X.; Hratchian, H. P.; Izmaylov, A. F.; Bloino, J.; Zheng, G.; Sonnenberg, J. L.; Hada, M.; Ehara, M.; Toyota, K.; Fukuda, R.; Hasegawa, J.; Ishida, M.; Nakajima, T.; Honda, Y.; Kitao, O.; Nakai, H.; Vreven, T.; J. A. Montgomery, J.; Peralta, J. E.; Ogliaro, F.; Bearpark, M.; Heyd, J. J.; Brothers, E.; Kudin, K. N.; Staroverov, V. N.; Keith, T.; Kobayashi, R.; Normand, J.; Raghavachari, K.; Rendell, A.; Burant, J. C.; Iyengar, S. S.; Tomasi, J.; Cossi, M.; Rega, N.; Millam, J. M.; Klene, M.; Knox, J. E.; Cross, J. B.; Bakken, V.; Adamo, C.; Jaramillo, J.; Gomperts, R.; Stratmann, R. E.; Yazyev, O.; Austin, A. J.; Cammi, R.; Pomelli, C.; Ochterski, J. W.; Martin, R. L.; Morokuma, K.; Zakrzewski, V. G.; Voth, G. A.; Salvador, P.; Dannenberg, J. J.; Dapprich, S.; Daniels, A. D.; Farkas, O.; Foresman, J. B.; Ortiz, J. V.; Cioslowski, J.; Fox, D. J. *Gaussian 09*, Revision D.1; Gaussian, Inc.: Pittsburgh PA, **2013**.
2. Mennucci, B.; Tomasi, J.; Cammi, R.; Cheeseman, J. R.; Frisch, M. J.; Devlin, F. J.; Gabriel, S.; Stephens, P. J., Polarizable continuum model (PCM) calculations of solvent effects on optical rotations of chiral molecules. *J. Phys. Chem. A* **2002,** *106* (25), 6102-6113.
3. Grimme, S.; Antony, J.; Ehrlich, S.; Krieg, H., A consistent and accurate ab initio parametrization of density functional dispersion correction (DFT-D) for the 94 elements H-Pu. *J. Chem. Phys.* **2010,** *132* (15), 154104.
4. Roy, L. E.; Hay, P. J.; Martin, R. L., Revised Basis Sets for the LANL Effective Core Potentials. *J. Chem. Theory Comput.* **2008,** *4* (7), 1029-31.
5. Lu, T.; Chen, F., Multiwfn: a multifunctional wavefunction analyzer. *J. Comput. Chem.* **2012,** *33* (5), 580-92.
6. Lu, T.; Chen, F., Quantitative analysis of molecular surface based on improved Marching Tetrahedra algorithm. *J. Mol. Graph. Model.* **2012,** *38*, 314-23.
7. For $\mathbf{1}^{3+}$, when the basis set superposition error correction (BSSE) was considered to estimate the ΔE_{HG}, the binding order is almost preserved ($H_2PO_4^-$ > HSO_4^- > ClO_4^- > CH_3COO^- > NO_3^-), with acetate and perchlorate exchanging positions. Still, this binding affinity preference does not mirror the binding order built with the ^{1}H NMR experimental data. Therefore, and given the large number of structures to be re-optimized, we decided to not extend the BSSE calculations to the remaining host's oxidation states.
8. Bader, R. F. W., *Atoms in Molecules: A Quantum Theory*. Oxford University Press: 1991.
9. Weinhold, F.; Landis, C. R., Natural Bond Orbitals and Extensions of Localized Bonding Concepts. *Chem. Educ. Res. Pract.* **2001,** *2* (2), 91-104.
10. Glendening, E. D.; Landis, C. R.; Weinhold, F., NBO 6.0: natural bond orbital analysis program. *J. Comput. Chem.* **2013,** *34* (16), 1429-37.
11. Espinosa, E.; Molins, E.; Lecomte, C., Hydrogen bond strengths revealed by topological analyses of experimentally observed electron densities. *Chem. Phys. Lett.* **1998,** *285* (3-4), 170-173.
12. Koopmans, T., Über die Zuordnung von Wellenfunktionen und Eigenwerten zu den Einzelnen Elektronen Eines Atoms. *Physica* **1934,** *1* (1-6), 104-113.
13. Petrushenko, I. K., DFT Study on Adiabatic and Vertical Ionization Potentials of Graphene Sheets. *Advances in Materials Science and Engineering* **2015,** *2015*, 1-7.

Commented [JRBG20]: Usually, full ref. 1 is provided in the SI while in the main text it is given a short version with one author followed by et al.